

Semi-analytical steady-state response prediction for multi-dimensional quasi-Hamiltonian systems

Wen-Wei Ye(叶文伟), Lin-Cong Chen(陈林聪), Zi Yuan(原子), Jia-Min Qian(钱佳敏), and Jian-Qiao Sun(孙建桥)
Citation: Chin. Phys. B, 2023, 32 (**6**): 060506. DOI: 10.1088/1674-1056/acae7c
Journal homepage: http://cpb.iphy.ac.cn; http://iopscience.iop.org/cpb

What follows is a list of articles you may be interested in

Detecting physical laws from data of stochastic dynamical systems perturbed by non-Gaussian α-stable Lévy noise

Linghongzhi Lu(陆凌弘志), Yang Li(李扬), and Xianbin Liu(刘先斌)
Chin. Phys. B, 2023, 32 (**5**): 050501. DOI: 10.1088/1674-1056/aca7ee

Data-driven modeling of a four-dimensional stochastic projectile system

Yong Huang(黄勇) and Yang Li(李扬)
Chin. Phys. B, 2022, 31 (**7**): 070501. DOI: 10.1088/1674-1056/ac4e0d

Intrinsic fluctuation and susceptibility in somatic cell reprogramming process

Jian Shen(沈健), Xiaomin Zhang(张小敏), Qiliang Li(李齐亮), Xinyu Wang(王歆宇), Yunjie Zhao(赵蕴杰), Ya Jia(贾亚)
Chin. Phys. B, 2019, 28 (**4**): 040503. DOI: 10.1088/1674-1056/28/4/040503

Stochastic bifurcations of generalized Duffing-van der Pol system with fractional derivative under colored noise

Wei Li(李伟), Mei-Ting Zhang(张美婷), Jun-Feng Zhao(赵俊锋)
Chin. Phys. B, 2017, 26 (**9**): 090501. DOI: 10.1088/1674-1056/26/9/090501

Principal resonance response of a stochastic elastic impact oscillator under nonlinear delayed state feedback

Huang Dong-Mei (黄冬梅), Xu Wei (徐伟), Xie Wen-Xian (谢文贤), Han Qun (韩群)
Chin. Phys. B, 2015, 24 (**4**): 040502. DOI: 10.1088/1674-1056/24/4/040502

Semi-analytical steady-state response prediction for multi-dimensional quasi-Hamiltonian systems

Wen-Wei Ye(叶文伟)[1,2], Lin-Cong Chen(陈林聪)[1,2,†], Zi Yuan(原子)[1,2], Jia-Min Qian(钱佳敏)[1,2], and Jian-Qiao Sun(孙建桥)[3]

[1] *College of Civil Engineering, Huaqiao University, Xiamen* 361021, *China*
[2] *Key Laboratory for Intelligent Infrastructure and Monitoring of Fujian Province, Huaqiao University, Xiamen* 361021, *China*
[3] *Department of Mechanical Engineering School of Engineering, University of California Merced, CA* 95343, *USA*

(Received 14 October 2022; revised manuscript received 6 December 2022; accepted manuscript online 27 December 2022)

The majority of nonlinear stochastic systems can be expressed as the quasi-Hamiltonian systems in science and engineering. Moreover, the corresponding Hamiltonian system offers two concepts of integrability and resonance that can fully describe the global relationship among the degrees-of-freedom (DOFs) of the system. In this work, an effective and promising approximate semi-analytical method is proposed for the steady-state response of multi-dimensional quasi-Hamiltonian systems. To be specific, the trial solution of the reduced Fokker–Plank–Kolmogorov (FPK) equation is obtained by using radial basis function (RBF) neural networks. Then, the residual generated by substituting the trial solution into the reduced FPK equation is considered, and a loss function is constructed by combining random sampling technique. The unknown weight coefficients are optimized by minimizing the loss function through the Lagrange multiplier method. Moreover, an efficient sampling strategy is employed to promote the implementation of algorithms. Finally, two numerical examples are studied in detail, and all the semi-analytical solutions are compared with Monte Carlo simulations (MCS) results. The results indicate that the complex nonlinear dynamic features of the system response can be captured through the proposed scheme accurately.

Keywords: steady-state response, quasi-Hamiltonian systems, FPK equation, RBF neural networks

PACS: 05.10.–a, 05.10.Gg, 05.10.Ln, 05.40.–a **DOI:** 10.1088/1674-1056/acae7c

1. Introduction

The phenomena of random vibration are universal and their dynamic characteristics can be explained only by probability or statistics.[1,2] Most of practical engineering systems subjected to random loads can be described as a dissipative Hamiltonian system with random excitations, *i.e.*, quasi-Hamiltonian system.[3] The properties of quasi-Hamiltonian system, involving integrability and resonance, seriously affect the functional form and characteristics of the solution of the whole system. Hence, in-depth research of the quasi-Hamiltonian system is vital in solving real-world issues, such as the response, reliability, stability, bifurcation, and stochastic dynamic control. In fact, since the 1990s, Zhu and his team[4] have conducted a lot of researches of nonlinear stochastic dynamics and control in the framework of Hamiltonian systems. At present, the study of stochastic dynamics of quasi-Hamiltonian systems is still in the ascendant trend, which belongs to the frontier and hottest field of theoretical research of nonlinear stochastic dynamics.

With regards to the prediction of steady-state response, one has made great efforts for it because of its importance in the safety and reliability evaluation of structures. Nevertheless, only a few systems[5–7,9] allow exact solutions under strict conditions. Alternatively, some approximate or numerical analysis solutions are sought mainly for predicting the response to quasi-Hamiltonian systems. In accordance with three equivalent criteria that minimize the difference between systems statistically, the method of equivalent nonlinear (EQNL) system was developed to obtain the approximate steady-state probability density function (PDF) for multi-degree-of-freedom (MDOF) quasi-Hamiltonian systems driven by Gaussian white noises.[10,11] However, the application scope of this method still has some limitations, mainly because it needs enough nonlinear stochastic dynamic systems with exact steady-state solutions as a potential of the EQNL system. As an important approach to dealing with nonlinear random systems, stochastic averaging method was widely employed in the MDOF quasi-Hamiltonian systems under various excitations.[12–15] Notably, stochastic averaging method can effectively realize the dimensionality reduction for most systems, but it requires the correlation time of excitation to be much shorter than the relaxation time of the system. Thus, there is still a huge gap that needs to be further explored and improved.

There are many other approximate methods reported in the literature, which are possible to be applied to solving the problem of response of quasi-Hamiltonian systems, including cell mapping method,[16,17] exponential-polynomial-closure (EPC) approach,[18,19] and deep learning.[20–22] These

†Corresponding author. E-mail: lincongchen@hqu.edu.cn
© 2023 Chinese Physical Society and IOP Publishing Ltd

approaches mentioned above have their advantages and shortcomings. For example, the cell mapping method represents the relationship between state transitions in a dynamic system using discrete cell transitions, once the cell size is large, it will frequently create erroneous solutions and sometimes even cause significant mistakes. The EPC approach may produce highly accurate approximations for some nonlinear systems, while the weight function is built by using the Gaussian PDF, which severely restricts its application space. Deep learning can theoretically map to any function and has many layers and breadths, making it capable of resolving complex issues. However, deep learning frequently requires the assistance of enormous data, and the training period is lengthy to reach acceptable accuracy. Besides, Monte Carlo simulation (MCS)[23,24] is widely used as a general and effective statistical method, but it is often accompanied by expensive computing costs.

Striving for more accurate and efficient response analysis methods with wider range of applications has always been a common goal. Chen and Sun[25] developed a highly efficient method of iterative weighted residuals for MDOF nonlinear systems. The trial stationary PDF solution of the multi-dimensional system was constructed with the probabilistic potentials and polynomials. This method can effectively capture the main nonlinear characteristics of the steady-state response. However, it might be a challenge to acquire the marginal-probability-density-functions (mPDFs) for high-dimensional systems since the form of exponential polynomial is difficult to integrate, and the resonance problem of the system remains unsolved. More recently, Li *et al.*[26] innovatively combined the idea of stochastic averaging with data-driven identification technique to reduce the dimensionality of a nonlinear stochastic system, it partially addresses the shortcomings of both existing data-driven identification techniques and stochastic averaging methods while keeping their benefits, but it cannot be ignored either that the application of the maximum information entropy principle greatly increases the amount of calculation.

On the other hand, owing to the development of computer technology, many algorithms of neural networks arise at the historic moment and have attracted broad attention.[27–32] Among them, RBF neural networks have shown great computational superiority in solving various partial differential equations,[33–36] especially the FPK equation.[37,38] Wang *et al.* proposed the use of the RBF neural networks to calculate the transient solutions of FPK equations[38] and first-passage problems[37] in random vibrations, setting up a great wave of solving nonlinear random vibration problems. It is inspiring that the solution of the PDFs benefits greatly from the integrability of the Gaussian basis function. The RBF neural networks can theoretically achieve a particularly good fitting for any continuous functions with high precision, by increasing the number of hidden layer nodes on the basis of simple three-layer structure. Comparing with the simulation results, the accuracy of the solutions obtained in the higher dimensional case is apparently lower than those obtained in the lower dimensional case, partly because of limitations in computing memory; it is a challenge to gather enough data points for a satisfactory fit. To this end, an efficient sampling strategy is utilized in this paper to reduce unnecessary data points.

In this work, the RBF neural networks are extended to determine the steady PDFs of multi-dimensional quasi-Hamiltonian systems subjected to Gaussian white noise. Firstly, the RBF neural networks with undetermined weight coefficients are employed for constructing the trial stationary PDF solution. Then, a loss function is constructed by combining the random sampling technique around the residual generated in the FPK equation. Finally, the optimal weight coefficients can be obtained by minimizing the loss function with the help of the method of Lagrange multiplier. An efficient sampling strategy is proposed for selecting representative point set. To demonstrate the feasibility of the proposed scheme, two quasi-Hamiltonian systems are investigated, and the influences of some system parameters are further investigated.

2. Mathematical formulation

Consider a quasi-Hamiltonian system with n degrees-of-freedom, which random excitations act on, the equations of motion can be described as the following general form:[3]

$$\begin{aligned}&\frac{\mathrm{d}Q_j}{\mathrm{d}t}=\frac{\partial \hat{H}}{\partial P_j},\\&\frac{\mathrm{d}P_j}{\mathrm{d}t}=-\left[\frac{\partial \hat{H}}{\partial Q_j}+f_{ij}\frac{\partial \hat{H}}{\partial P_i}\right]+g_{jl}W_l(t),\\&i,j=1,2,\ldots,n;\quad l=1,2,\ldots,m,\end{aligned}\tag{1}$$

where Q_j and P_j respectively denote the generalized displacement and generalized velocity of the j-th degree-of-freedom system, $\hat{H}=\hat{H}(q_1,q_2,\ldots,q_n,p_1,p_2,\ldots,p_n)$ represents the Hamiltonian function of the undisturbed Hamiltonian system, $f_{ij}=f_{ij}(q_1,q_2,\ldots,q_n,p_1,p_2,\ldots p_n)$ are defined as the coefficients of damping terms, $g_{jl}=g_{jl}(q_1,q_2,\ldots q_n,p_1,p_2,\ldots,p_n)$ represent amplitude functions of the random excitations, and $W_l(t)$ are a set of zero-mean Gaussian white noises with cross-correlation $E[W_l(t)W_s(t+\tau)]=2D_{ls}(\tau)$, $l,s=1,2,\ldots,m$.

Subsequently, the Itô equation corresponding to Eq. (1) reads

$$\begin{aligned}&\mathrm{d}Q_j=\frac{\partial \hat{H}}{\partial P_j}\mathrm{d}t,\\&\mathrm{d}P_j=\left[-\frac{\partial \hat{H}}{\partial Q_j}-f_{ij}\frac{\partial \hat{H}}{\partial P_i}+D_{ls}g_{is}\frac{\partial g_{jl}}{\partial P_i}\right]\mathrm{d}t+\sigma_{jl}\,\mathrm{d}B_l(t),\\&i,j=1,2,\ldots,n;\quad l=1,2,\ldots,m,\end{aligned}\tag{2}$$

where $\sigma_{jl} = (\boldsymbol{gL})_{jl}$, $\boldsymbol{g} = [g_{il}]_{n\times m}$, $\boldsymbol{LL}^{\mathrm{T}} = 2\boldsymbol{D}$, and B_l(t) represents the Wiener process. Notably, the correction terms of Wong–Zakai $D_{ls}g_{is}\partial g_{jl}/\partial P_i$ can usually be divided into conservative part and dissipative part, then merging these two parts with $-\partial\hat{H}/\partial Q_j$ and $f_{ij}\partial\hat{H}/\partial P_i$, respectively, equation (2) can be recast as

$$\begin{aligned} \mathrm{d}Q_j &= \frac{\partial H}{\partial P_j}\mathrm{d}t, \\ \mathrm{d}P_j &= -\left[\frac{\partial H}{\partial Q_j} + m_{ij}\frac{\partial H}{\partial P_j}\right]\mathrm{d}t + \sigma_{jl}\,\mathrm{d}B_l(t), \end{aligned} \tag{3}$$

in which $H = H(q_1, q_2, \ldots, q_n, p_1, p_2, \ldots p_n)$ denotes the modified Hamiltonian function, and m_{ij} represent the modified damping terms.

The steady PDF, $\rho = \rho(\boldsymbol{q}, \boldsymbol{p})$, of system (1) is dominated by the following FPK equation when $\partial\rho/\partial t = 0$ vanishes:

$$\begin{aligned} &-\frac{\partial\rho}{\partial q_j} + \frac{\partial\rho}{\partial p_j} + \frac{\partial^2 H}{\partial p_j^2}(m_{ij}\rho) \\ &+\frac{\partial H}{\partial p_j}\frac{\partial(m_{ij}\rho)}{\partial p_j} + \frac{1}{2}\frac{\partial^2(b_{ij}\rho)}{\partial p_i\partial p_j} = \frac{\partial\rho}{\partial t}, \\ &i, j = 1, 2, \ldots, n, \end{aligned} \tag{4}$$

where $b_{ij} = 2D_{ls}g_{jl}g_{is}$ represent the diffusion coefficients.

In general, it is very hard to obtain the exact solution of the stationary FPK Eq. (4). Up to now, the exact solutions have been available only to a limited number of systems.[5–9] Especially for high-dimensional systems with coupled nonlinear terms, the solution is very difficult to achieve. If the techniques of reduced dimension, such as stochastic averaging method[12] and state-space-split approach,[39] are adopted instead, some coupled nonlinear terms would disappear, and it is difficult to reflect the energy exchange relationship between different degrees of freedom. In the next section, a semi-analytical scheme to deal with the reduced FPK Eq. (4) via RBF neural networks, namely the RBF-NN scheme, is presented.

3. Implementation of the RBF-NN scheme

The RBF-NN scheme can be decomposed into two processes: assuming the trial stationary PDF solution in the form of RBF neural networks and obtaining the optimal weight coefficients by minimizing the residual based on the least square principle. To reduce the computational burden, however, an efficient sampling strategy is proposed, thereby reducing the computational memory.

3.1. General frame of RBF neural networks

In this study, the multivariate Gaussian form[37] is adopted as the activation function of the RBF neural networks, which is defined as

$$G_j(\boldsymbol{x}, \boldsymbol{\mu}_j, \boldsymbol{\sigma}_j) = \prod_{i=1}^{2n}\frac{1}{\sqrt{2\pi\sigma_{j,i}^2}}\exp\left[-\frac{(x_i - \mu_{j,i})^2}{2\sigma_{j,i}^2}\right], \tag{5}$$

where $\boldsymbol{x} = (x_1, x_2, \ldots, x_{2n-1}, x_{2n}) = (q_1, p_1, \ldots, q_n, p_n) \in \mathbb{R}^{2n}$ is the position vector, $\boldsymbol{\mu}_j = (\mu_{j,1}, \mu_{j,2}, \ldots, \mu_{j,2n-1}, \mu_{j,2n}) \in \mathbb{R}^{2n}$ and $\boldsymbol{\sigma}_j = (\sigma_{j,1}, \sigma_{j,2}, \ldots, \sigma_{j,2n-1}, \sigma_{j,2n}) \in \mathbb{R}^{2n}$ denote the centers and the standard deviations of the multivariate Gaussian functions, respectively.

Let the trial PDF solution of the reduced FPK Eq. (4) be

$$\tilde{\rho}(\boldsymbol{x}, \boldsymbol{w}) = \sum_{j=1}^{N_{\mathrm{G}}} w_j G_j(\boldsymbol{x}, \boldsymbol{\mu}_j, \boldsymbol{\sigma}_j), \tag{6}$$

where $\boldsymbol{w} = [w_1, w_2, \ldots, w_{N_{\mathrm{G}}}]^{\mathrm{T}}$ is the vector of unknown weight coefficients w_j, and N_{G} is the number of multivariate Gaussian functions in central domain Ω_{G}. Note that MCS can be employed to roughly estimate the domain Ω_{G}. Since the trial RBF-NN solution $\tilde{\rho}$ with a fixed form cannot exactly satisfy the reduced FPK Eq. (4), by replacing ρ with $\tilde{\rho}$ in Eq. (4), a residual $\delta(\boldsymbol{x}, \boldsymbol{w})$ can be yielded as follows:

$$\begin{aligned} \delta(\boldsymbol{x}, \boldsymbol{w}) \;=\; &-\frac{\partial\tilde{\rho}}{\partial q_j} + \frac{\partial\tilde{\rho}}{\partial p_j} + \frac{\partial^2 H}{\partial p_j^2}(m_{ij}\tilde{\rho}) + \frac{\partial H}{\partial p_j}\frac{\partial(m_{ij}\tilde{\rho})}{\partial p_j} \\ &+\frac{1}{2}\frac{\partial^2(b_{ij}\tilde{\rho})}{\partial p_i\partial p_j}, \quad i, j = 1, 2, \ldots, n. \end{aligned} \tag{7}$$

Note that the optimal RBF-NN solution can be obtained if the residual $\delta(\boldsymbol{x}, \boldsymbol{w})$ is minimized in the domain Ω_{G}. Equation (7) can be rewritten in the following compact form:

$$\delta(\boldsymbol{x}, \boldsymbol{w}) = \sum_{j=1}^{N_{\mathrm{G}}} w_j s_j(\boldsymbol{x}), \tag{8}$$

where $s_j(\boldsymbol{x})$ is defined as

$$\begin{aligned} s_j(\boldsymbol{x}) \;=\; &-\frac{\partial G_j}{\partial q_j} + \frac{\partial G_j}{\partial p_j} + \frac{\partial^2 H}{\partial p_j^2}(m_{ij}G_j) + \frac{\partial H}{\partial p_j}\frac{\partial(m_{ij}G_j)}{\partial p_j} \\ &+\frac{1}{2}\frac{\partial^2(b_{ij}G_j)}{\partial p_i\partial p_j}, \quad i, j = 1, 2, \ldots, n. \end{aligned} \tag{9}$$

3.2. Optimization algorithm for minimizing residual

By adopting sampling technique, a loss function can be established as follows:

$$\mathrm{Loss}(\boldsymbol{w}) = \frac{1}{N_{\mathrm{S}}}\sum_{i=1}^{N_{\mathrm{S}}}\delta^2(\boldsymbol{x}_i, \boldsymbol{w}), \tag{10}$$

where N_{S} denotes the number of sample points in domain Ω_{S}. Notably, in the earlier work it was proved that it is beneficial to select Ω_{S} slightly larger than Ω_{G}.

The trial RBF-NN solution and multivariate Gaussian functions satisfy the normalization condition as follows:

$$\int_{\mathbb{R}^{2n}}\tilde{\rho}\,\mathrm{d}\boldsymbol{x} = 1, \tag{11}$$

$$\int_{\mathbb{R}^{2n}} G_j\,\mathrm{d}\boldsymbol{x} = 1, \quad \text{for all } j. \tag{12}$$

Then, a constraint on the weight coefficients w_j can be derived from Eqs. (11) and (12) and given by

$$\sum_{j=1}^{N_{\rm G}} w_j = 1. \tag{13}$$

A Lagrangian function $L_{\rm s}(\boldsymbol{w})$ that includes the constraint Eq. (13), is defined by using a Lagrange multiplier λ, specifically,

$$\begin{aligned} L_{\rm s}(\boldsymbol{w}) &= \frac{1}{N_{\rm S}}\sum_{i=1}^{N_{\rm S}} \delta^2(\boldsymbol{x}_i,\boldsymbol{w}) + \lambda\left(\sum_{j=1}^{N_{\rm G}} w_j - 1\right) \\ &= \frac{1}{N_{\rm S}}\sum_{i=1}^{N_{\rm S}}\sum_{k=1}^{N_{\rm G}}\sum_{l=1}^{N_{\rm G}} w_k s_k(\boldsymbol{x}_i) s_r(\boldsymbol{x}_i) w_r \\ &\quad + \lambda\left(\sum_{j=1}^{N_{\rm G}} w_j - 1\right). \end{aligned} \tag{14}$$

The necessary conditions for minimization of $L_{\rm s}(\boldsymbol{w})$ are given by

$$\begin{aligned} &\frac{\partial L_{\rm s}}{\partial w_k} = 0, \quad k = 1,2,\ldots,N_{\rm G}, \\ &\frac{\partial L_{\rm s}}{\partial \lambda} = \sum_{j=1}^{N_{\rm G}} w_j - 1 = 0. \end{aligned} \tag{15}$$

Let $\boldsymbol{c} = [\boldsymbol{w},\lambda]^{\rm T} = [w_1, w_2, \ldots, w_{N_{\rm G}}, \lambda]^{\rm T}$, $\boldsymbol{b} = [0,0,\ldots,0,1]^{\rm T} \in \mathbb{R}^{(N_{\rm G}+1)\times 1}$ and build a matrix as

$$\boldsymbol{A} = \begin{bmatrix} & & 1 \\ & \boldsymbol{S} & \vdots \\ & & 1 \\ 0 & \cdots & 0\ 0 \end{bmatrix} \in \mathbb{R}^{(N_{\rm G}+1)\times(N_{\rm G}+1)}, \tag{16}$$

where the data matrix $\boldsymbol{S}$ is expressed as

$$\boldsymbol{S} = [\boldsymbol{S}_{kl}] = \left[\frac{1}{N_{\rm S}}\sum_{i=1}^{N_{\rm S}} s_k(\boldsymbol{x}_i) s_l(\boldsymbol{x}_i)\right] \in \mathbb{R}^{N_{\rm G}\times N_{\rm G}}. \tag{17}$$

Thus, equation (14) can be recast as the matrix form below:

$$L_{\rm s}(\boldsymbol{c}) = \boldsymbol{c}^{\rm T}\boldsymbol{A}\boldsymbol{c} - \boldsymbol{c}^{\rm T}\boldsymbol{b}. \tag{18}$$

Accordingly, the necessary condition in Eq. (15) turns into

$$\frac{\partial L_{\rm s}}{\partial \boldsymbol{c}} = (\boldsymbol{A} + \boldsymbol{A}^{\rm T})\boldsymbol{c} - \boldsymbol{b} = 0, \tag{19}$$

which can be solved readily, and the result is given below:

$$\boldsymbol{c}^* = (\boldsymbol{A} + \boldsymbol{A}^{\rm T})^{-1}\boldsymbol{b}, \tag{20}$$

only if the inverse $(\boldsymbol{A} + \boldsymbol{A}^{\rm T})^{-1}$ exists, can the optimal weight coefficient vector $\boldsymbol{w}^*$ be obtained by eliminating the Lagrange multiplier λ. Actually, the existence of matrix inverse relies heavily on the data matrix $\boldsymbol{S}$.[40] It was proved that the singularity of inverse matrix could be avoided when $N_{\rm S} \gg N_{\rm G}$.

The minimum value of the residual can be determined by substituting $\boldsymbol{w}^*$ into Eq. (10), and is given below:

$$\begin{aligned} \delta^* &= \sqrt{\frac{1}{N_{\rm S}}\sum_{i=1}^{N_{\rm S}}\left(\sum_{k=1}^{N_{\rm G}}\sum_{l=1}^{N_{\rm G}} w_k s_k(\boldsymbol{x}_i) s_l(\boldsymbol{x}_i) w_l\right)} \\ &= \sqrt{\boldsymbol{w}^{*\rm T}\boldsymbol{S}\boldsymbol{w}^*} < \varepsilon, \end{aligned} \tag{21}$$

where ε refers to a preset residual according to the accuracy requirements.

Note that the data matrix S may be very large and thus occupy a large number of computational memories. To this end, an efficient screening strategy for representative point sets is a supplement to the RBF-NN scheme as discussed in the next subsection.

3.3. Efficient sampling strategy

Generally, with regard to the joint PDFs of the nonlinear random vibration system, the spatial distribution domain of the multi-dimensional random variables is spherically symmetric or approximately spherically symmetric, and exhibits approximate radiation attenuation.[41] In terms of this distributional property, the representative point sets can be screened in a hypersphere. The process is outlined briefly below.

(i) First, two τ-dimensional unit hypercube domains ($\boldsymbol{H}_{\rm S}$ and $\boldsymbol{H}_{\rm C}$) are generated. Then $\boldsymbol{H}_{\rm C}$ is divided into $N_{\rm G0} = (n_{\rm c})^\tau$ grids, while $\boldsymbol{H}_{\boldsymbol{S}}$ is discretized into $N_{\rm S0} = (n_{\rm s})^\tau$ grids, specifically,

$$\begin{aligned} &\vartheta_{j,k} \in [-1,1]^\tau, \quad j = 1,2,\ldots,\tau;\ k = 1,2,\ldots,N_{\rm G_0}, \\ &\theta_{j,l} \in [-1,1]^\tau, \quad j = 1,2,\ldots,\tau;\ l = 1,2,\ldots,N_{\rm S_0}, \end{aligned} \tag{22}$$

where $\theta_{j,k}$ and $\vartheta_{j,l}$ represent the initial unit point sets for the central points and sample points.

(ii) Select the points in $\vartheta_{j,k}$ and $\theta_{j,l}$, which meet the following constraint:

$$\sum_{j=1}^{\tau}\vartheta_{j,k}^2 \le 1, \quad \sum_{j=1}^{\tau}\theta_{j,l}^2 \le 1, \tag{23}$$

to constitute the representative point sets. Figure 1 shows the distribution of the representative point set when $\tau = 2$.

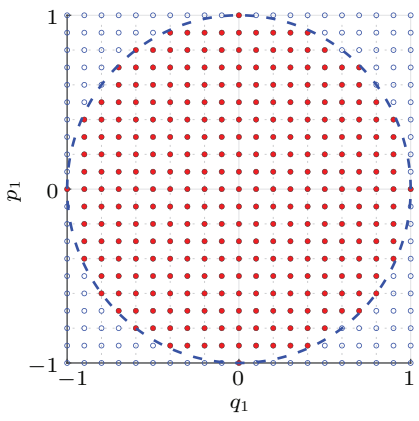


Fig. 1. Distribution of representative point set when $\tau = 2$, with symbols red • and blue ○ representing points inside and outside hypersphere, respectively.

To measure the screening effect of this sampling strategy, a screening ratio χ is defined as

$$\chi = \frac{N_{\mathrm{G}}}{N_{\mathrm{G}_0}} \quad \text{or} \quad \frac{N_{\mathrm{S}}}{N_{\mathrm{S}_0}}, \tag{24}$$

where N_{G} and N_{S} are the number of representative point sets for the central points and the sample points, respectively. It can be inferred that when the number of selected points is large enough, the screening ratio χ tends to a fixed value, that is, the ratio of the volume of unit hypersphere to unit hypercube, specifically,

$$\chi = \frac{V_\tau}{M_\tau} = \begin{cases} \dfrac{\pi^{\tau/2}}{2^\tau\left(\dfrac{\tau}{2}\right)!}, & \tau = 2,4,\ldots,2k, \\ \dfrac{\left(\dfrac{\tau-1}{2}\right)!\pi^{(\tau-1)/2}}{\tau!}, & \tau = 3,5,\ldots,2k+1, \end{cases} \tag{25}$$

where V_τ and M_τ denote the volume of the τ-dimensional hypersphere and the τ-dimensional hypercube, respectively.

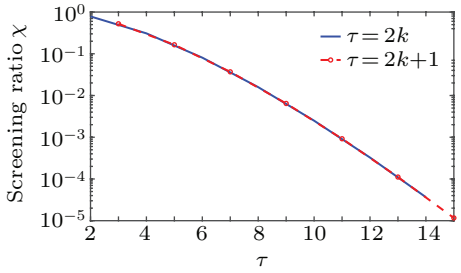


Fig. 2. Curves of ideal screening ratio χ *versus* τ in different dimensions.

In Fig. 2, the curves of screening ratios in different dimensions are depicted. It is worth noting that the screening effect is amazing, the screening strategy can greatly reduce the number of selected points, thereby reducing the computational burden of the data matrix $\boldsymbol{S}$ and improving the computational efficiency.

(iii) Let the representative point sets inside the hypersphere for the central points and sample points be $\hat{\vartheta}_\varphi = (\hat{\vartheta}_{1,\varphi}, \hat{\vartheta}_{2,\varphi}, \ldots, \hat{\vartheta}_{\tau,\varphi})$, $\phi = 1,2,\ldots,N_{\mathrm{G}}$, and $\hat{\theta}_\phi = (\hat{\theta}_{1,\phi}, \hat{\theta}_{2,\phi}, \ldots, \hat{\theta}_{\tau,\phi})$, $\varphi = 1,2,\ldots,N_{\mathrm{S}}$, respectively. According to the domain size of the central points and sample points, the scaling transformation is performed on the unit hyperspherical point sets, *i.e.*,

$$\begin{aligned} \boldsymbol{\mu}_{j,\varphi} &= \hat{\vartheta}_{j,\varphi}\alpha_j = (\hat{\vartheta}_{1,\varphi}\alpha_1, \hat{\vartheta}_{2,\varphi}\alpha_2, \ldots, \hat{\vartheta}_{\tau,\varphi}\alpha_\tau), \\ \boldsymbol{x}_{j,\phi} &= \hat{\theta}_{j,\phi}\beta_j = (\hat{\theta}_{1,\phi}\beta_1, \hat{\theta}_{2,\phi}\beta_2, \ldots, \hat{\theta}_{\tau,\phi}\beta_\tau). \end{aligned} \tag{26}$$

The implementation of the proposed RBF-NN scheme combined with efficient sampling strategy is sketched in Algorithm 1. Note that the optimization algorithm converts the solving problem of the unknown weight coefficient in Eq. (6) into a simple matrix operation. Thus, the solution of the higher-dimensional FPK equation can be obtained in the semi-analytical form. Though the worst time complexity is $O((N_{\mathrm{G}})^2 N_{\mathrm{S}})$ and the worst space complexity is $O(N_{\mathrm{G}}N_{\mathrm{S}})$, which depend to a large extent on the number of selected central points and sample points, *i.e.*, N_{G} and N_{S}. Then the suggested sampling strategy can reduce the complexity to some extent, as indicated in Fig. 2. More importantly, it provides a new perspective in solving high-dimensional FPK equations, and the validity of this algorithm will be tested in the next section.

Algorithm 1 RBF-NN algorithm

Input: the central point sets with initial number of $N_{\mathrm{G}0} = (n_{\mathrm{c}})^\tau$ in the central domain $[-\alpha_i, \alpha_i]^\tau$, the sample point sets with initial number of $N_{\mathrm{S}0} = (n_{\mathrm{s}})^\tau$ in the sample domain $[-\beta_i, \beta_i]^\tau$, and the covariance of the multivariate Gaussian functions $\boldsymbol{\sigma}_j$ is taken as the grid width of the j-th dimension of the central domain.

Output: weight coefficients w_j, the RBF-NN PDFs.

1: Generate source nodes and screen the point sets in hypercube spheres

$\vartheta_{j,k} \in [-1,1]^\tau$, $\quad j = 1,2,\ldots,\tau,\ k = 1,2,\ldots,N_{\mathrm{G}_0}$,

when $\sum_{j=1}^{\tau} \vartheta_{j,k}^2 \le 1 \Rightarrow \hat{\vartheta}_{j,\varphi}$, $\quad \varphi = 1,2,\ldots,N_{\mathrm{G}}$;

$\theta_{j,l} \in [-1,1]^\tau, j = 1,2,\ldots,\tau$, $\quad l = 1,2,\ldots,N_{\mathrm{S}_0}$,

when $\sum_{j=1}^{\tau} \theta_{j,l}^2 \le 1 \Rightarrow \hat{\theta}_{j,\phi}$, $\quad \phi = 1,2,\ldots,N_{\mathrm{S}}$.

2: Scale transformation is performed on the screening point sets, *i.e.*,

$\boldsymbol{\mu}_{j,\varphi} = \hat{\vartheta}_{j,\varphi}\alpha_j = (\hat{\vartheta}_{1,\varphi}\alpha_1, \hat{\vartheta}_{2,\varphi}\alpha_2, \ldots, \hat{\vartheta}_{\tau,\varphi}\alpha_\tau)$,

$\boldsymbol{x}_{j,\phi} = \hat{\theta}_{j,\phi}\beta_j = (\hat{\theta}_{1,\phi}\beta_1, \hat{\theta}_{2,\phi}\beta_2, \ldots, \hat{\theta}_{\tau,\phi}\beta_\tau)$.

3: Assume the trial solution of FPK equation as $\tilde{\rho}(\boldsymbol{x}, \boldsymbol{w}) = \sum_{j=1}^{N_{\mathrm{G}}} w_j G_j(\boldsymbol{x}, \boldsymbol{\mu}_j, \boldsymbol{\sigma}_j)$.

4: Construct the loss function $\mathrm{Loss}(\boldsymbol{c}) = \frac{1}{N_{\mathrm{S}}} \sum_{i=1}^{N_{\mathrm{S}}} \delta^2(\boldsymbol{x}_i, \boldsymbol{w})$.

5: Introduce Lagrange multiplier method for optimization

$$L_{\mathrm{s}}(\boldsymbol{c}) = \frac{1}{N_{\mathrm{S}}} \sum_{i=1}^{N_{\mathrm{S}}} \delta^2(\boldsymbol{x}_i, \boldsymbol{w}) + \lambda\left(\sum_{j=1}^{N_{\mathrm{G}}} w_j - 1\right) = \boldsymbol{c}^{\mathrm{T}}\boldsymbol{A}\boldsymbol{c} - \boldsymbol{c}^{\mathrm{T}}\boldsymbol{b}.$$

6: Minimize the approximate square error $\frac{\partial L_{\mathrm{s}}}{\partial \boldsymbol{c}} = (\boldsymbol{A} + \boldsymbol{A}^{\mathrm{T}})\boldsymbol{c} - \boldsymbol{b} = 0$.

7: Solve the linear matrix equation $\boldsymbol{c}^* = (\boldsymbol{A} + \boldsymbol{A}^{\mathrm{T}})^{-1}\boldsymbol{b}$.

8: Estimate and verify the approximate residual $\delta^* = \sqrt{\boldsymbol{w}^{*\mathrm{T}}\boldsymbol{S}\boldsymbol{w}^*} < \varepsilon$.

4. Illustrative examples

Two specific nonlinear dynamical systems are investigated in this section. By comparing with the MCS results, the validity of the semi-analytical solutions and the feasibility of the proposed RBF-NN scheme are pointed out. Note that all the MCS results for comparison are conducted with a sample size of 5.0×10^8.

Example 1

As the first example, two nonlinearly and asymmetrically coupled Duffing systems[37] subjected to Gaussian white noises are considered, the equations of motion are described below:

$$\begin{cases} \dot{Q}_1=\dfrac{\partial H}{\partial P_1},\ \ \dot{P}_1=-\dfrac{\partial H}{\partial Q_1}-\mu_1\dfrac{\partial H}{\partial P_1}+W_1(t), \\ \dot{Q}_2=\dfrac{\partial H}{\partial P_2},\ \ \dot{P}_2=-\dfrac{\partial H}{\partial Q_2}-\mu_2\dfrac{\partial H}{\partial P_2}+W_2(t), \end{cases} \tag{27}$$

where $W_1(t)$ and $W_2(t)$ are two independent and zero-mean Gaussian white noises with intensity $2D_i$ ($i=1,\ 2$), and the Hamiltonian function H is

$$H=\frac{1}{2}(P_1^2+P_2^2)+U(Q_1,Q_2),$$

$$U(Q_1,Q_2)=\frac{1}{2}(\omega_1^2Q_1^2+\omega_2^2Q_2^2)+\frac{1}{4}(k_1Q_1^4+k_2Q_2^4)$$

$$-k_3Q_1Q_2-\frac{1}{3}k_4Q_1^3Q_2. \tag{28}$$

System (27) has a broad engineering application background, such as describing the navigation of ships and the operation of aerospace equipment. In accordance with Ref. [37], the parameters of the system (27) are dimensionless and set as follows: $\mu_1=0.2$, $\mu_2=0.2$, $\omega_1=0.2$, $\omega_2=0.4$, $k_1=0.3$, $k_2=0.5$, $k_3=0.3$, $k_4=0.12$, and Gaussian excitation intensity $2D_i=0.05$. Obviously, the Hamiltonian is not separable, then system (27) is non-integrable.

The central domain is selected as $\Omega_{\rm G}=[-2.5,2.5]\times[-1.5,1.5]\times[-2,2]\times[-1.5,1.5]$, which is evenly divided into $16\times16\times16\times16$ grids, and the sample domain is selected as $\Omega_{\rm S}=[-5,5]\times[-3,3]\times[-4,4]\times[-3,3]$, which is evenly divided into $32\times32\times32\times32$ grids. The standard deviation of the multivariate Gaussian function is uniformly taken as the grid size in the corresponding dimension of $\Omega_{\rm G}$, *i.e.*, $\sigma_j=[5/16,3/16,1/4,3/16]$. Subsequently, by adopting the efficient screening strategy, 15456 central points and 283872 sample points are retained respectively, *i.e.*, $N_{\rm G}=15456$ and $N_{\rm S}=283872$, the screening ratios are $\chi_{\rm G}=23.58\%$ and $\chi_{\rm S}=27.07\%$, respectively.

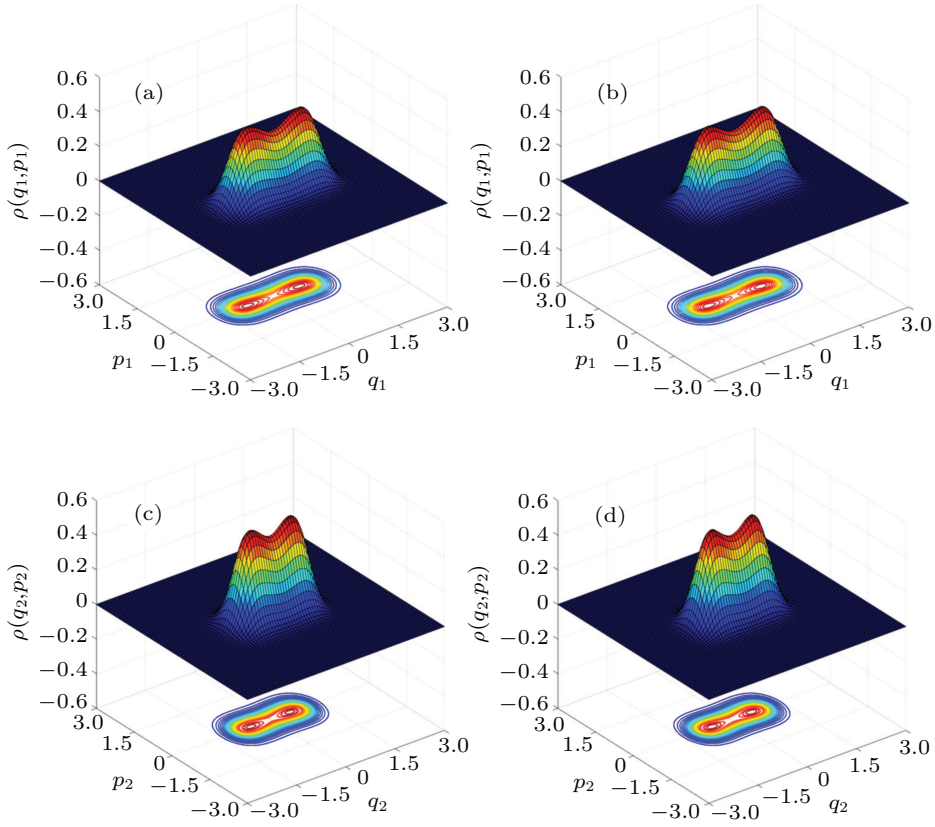


Fig. 3. Comparison among joint PDFs of system (27), showing [(a), (c)] RBF-NN solutions, and [(b), (d)] MCS results.

The semi-analytical solutions obtained by the RBF-NN scheme are all displayed in Fig. 3, and the MCS results are also presented to verify RBFNN solutions accordingly. As shown in Fig. 3, there is a double peak phenomenon for the joint PDFs of system (27) at each degree-of-freedom and the steady-state response of system (27) exhibits complex nonlin-

ear characteristics. Even so, the RBF-NN solutions are almost identical to the MCS results. Besides, the approximate residual δ^* is 2.316×10^{-4} and root-mean-square (RMS) error is 3.527×10^{-4}. The RBF-NN scheme consumes about 3138 s of the CPU time which is still much faster than 4.0 h consumed by the MCS.

Further, the influence of the ratio between the constant damping terms, μ_1 and μ_2, on the system response is investigated. Through the proposed scheme, when $\mu_1 = 0.2$ and $\mu_2 = 0.5\mu_1$, $1.0\mu_1$, $2.0\mu_1$, the RBF-NN solutions compared with the MCS results are depicted in Fig. 4. Apparently, it is observed that the mPDFs of displacement are bimodal while those of velocity are unimodal, and the peaks of the marginal PDFs become higher and sharper as μ_2 increases. It means that system (27) is prone to local offset and this tendency will be promoted as μ_2 increases, even though the increase of damping inhibits the velocity. More importantly, all the results obtained by the RBF-NN scheme are quite consistent with those obtained by the MCS.

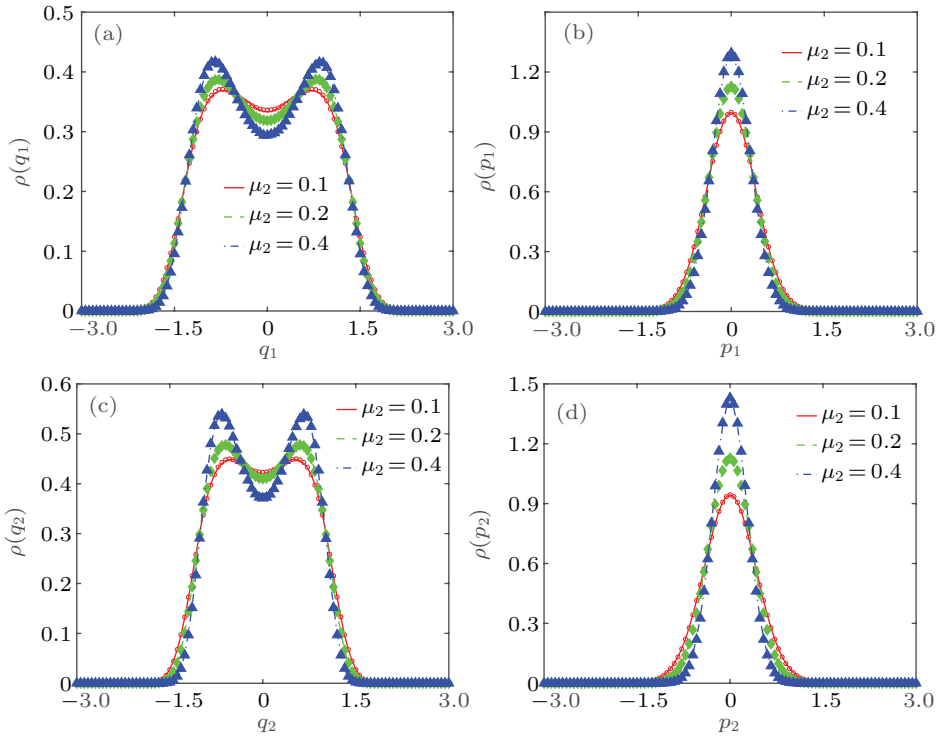


Fig. 4. Curves of mPDFs of system (27) for three different values of μ_2, with color lines denoting RBF-NN solutions, and symbols (◯, ◊, △) representing MCS results.

Example 2

The second example illustrates two nonlinear oscillators[42] with nonlinear coupling damping under Gaussian white noise excitations, and the equations of motion are established as follows:

$$\begin{cases} \dot{Q}_1 = \dfrac{\partial H}{\partial P_1}, \\ \dot{P}_1 = -\dfrac{\partial H}{\partial Q_1} - (\alpha_{10}+\alpha_{11}P_1^2+\alpha_{12}P_2^2)\dfrac{\partial H}{\partial P_1} \\ \qquad -\alpha_{13}\dfrac{\partial H}{\partial P_2} + W_1(t), \\ \dot{Q}_2 = \dfrac{\partial H}{\partial P_2}, \\ \dot{P}_2 = -\dfrac{\partial H}{\partial Q_2} - (\alpha_{20}+\alpha_{21}P_1^2+\alpha_{22}P_2^2)\dfrac{\partial H}{\partial P_2} \\ \qquad -\alpha_{23}\dfrac{\partial H}{\partial P_1} + W_2(t), \end{cases} \tag{29}$$

where $W_1(t)$ and $W_2(t)$ are two independent and zero-mean Gaussian white noises with intensity $2D_i$ ($i = 1, 2$), and the Hamiltonian function

$$H = \frac{1}{2}(P_1^2+P_2^2+\omega_1^2Q_1^2+\omega_2^2Q_2^2). \tag{30}$$

To explore the rich dynamic characteristics, the dimensionless system parameters are in a reasonable range and listed as follows: $\alpha_{10}=0.2$, $\alpha_{20}=0.1$, $\alpha_{30}=0.2$, $\alpha_{11}=0.3$, $\alpha_{21}=0.4$, $\alpha_{31}=0.5$, $\alpha_{12}=0.12$, $\alpha_{22}=0.1$, $\alpha_{32}=0.12$, $\alpha_{13}=0.4$, $\alpha_{23}=0.3$, and Gaussian excitation intensity $2D_i=0.1$. System (29) is quasi-integrable. The non-resonant case and resonant case are analyzed separately below.

Case 1: Non-resonant case

When $\omega_1 = 1.0$ and $\omega_2 = \sqrt{2}$, system (29) is in non-resonance. In this case, the central domain is selected as $\Omega_G = [-1.5,1.5]\times[-1.5,1.5]\times[-1.5,1.5]\times[-1,1]\times[-1.5,1.5]$ meshed into $16\times16\times16\times16$ grids, and the sample domain is selected as $\Omega_S = [-3,3]\times[-3,3]\times[-2,2]\times[-3,3]$ meshed into $32\times32\times32\times32$ grids. The values of standard devi-

ation σ_j are equably set to the grid size on each dimension of $\Omega_{\rm G}$, *i.e.*, $\sigma_j = [3/16, 3/16, 1/8, 3/16]$, Then 15456 central points and 283872 sample points are respectively kept unchanged in computing by using the efficient screening strategy, *i.e.*, $N_{\rm G} = 15456$ and $N_{\rm S} = 283872$, the screening ratios are $\chi_{\rm G} = 23.58\%$ and $\chi_{\rm S} = 27.07\%$, respectively.

The semi-analytical solutions attained by using the proposed scheme are displayed in Fig. 5, and compared with the corresponding MCS results. It is clear from Fig. 5 that the semi-analytical solutions coincide with the MCS results. The approximate residual δ^* was 2.316×10^{-4} and RMS error was 9.019×10^{-4}, which were acceptable. The CPU time consumes about 3259 s, less than about 4.0 h consumed by MCS. The proposed scheme shows high accuracy and relatively high efficiency.

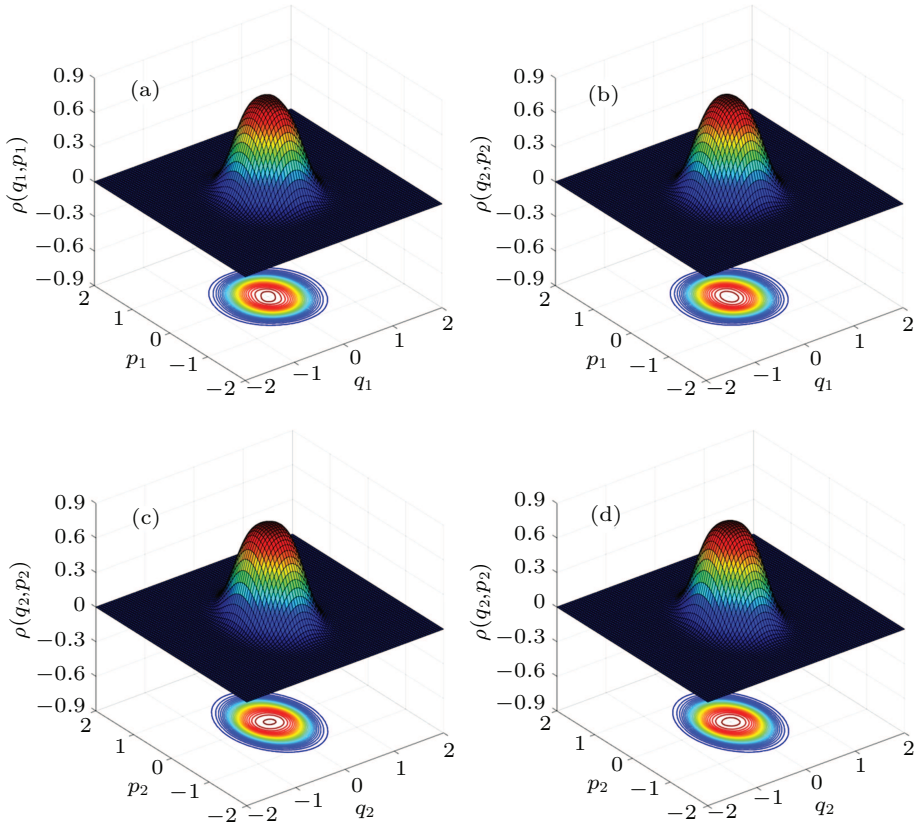


Fig. 5. Comparison among joint PDFs of system (29) in non-resonance, showing [(a), (c)] RBF-NN solutions and [(b), (d)] MCS results.

Case 2: Resonant case

When $\omega_1 = \omega_2 = 1.0$, system (29) is in resonance. Similarly, the central domain is selected as $\Omega_{\rm G} = [-1.5, 1.5] \times [-1.5, 1.5] \times [-1.5, 1.5] \times [-1.5, 1.5]$ meshed into $18 \times 18 \times 18 \times 18$ grids, and the sample domain is selected as $\Omega_{\rm S} = [-3, 3] \times [-3, 3] \times [-3, 3] \times [-3, 3]$ meshed into $36 \times 36 \times 36 \times 36$ grids. The values of standard deviation σ_j are equably set to the grid size on each dimension of $\Omega_{\rm G}$, *i.e.*, $\sigma_j = [1/6, 1/6, 1/6, 1/6]$. Then 25472 central points and 462672 sample points are respectively kept unchanged in computing by using the efficient screening strategy, *i.e.*, $N_{\rm G} = 25472$ and $N_{\rm S} = 462672$, the screening ratios are $\chi_{\rm G} = 24.26\%$ and $\chi_{\rm S} = 27.55\%$, respectively.

The acquired semi-analytical RBF-NN solutions are indicated in Fig. 6. By comparing with the corresponding MCS results, the accuracy of the RBF-NN scheme is satisfactory that the approximate residual δ^* is about 5.452×10^{-4} and the RMS error is about 9.713×10^{-4}, the complex nonlinear response characteristics of the system (29) in resonant state can be well captured. Notably, the CPU time consumed by this example is about 10726 s, which is still less than 4.0 h spent by MCS, but it cannot be ignored in that the CPU time consumed increases significantly as the number of points taken on each dimension increases, where the influence of dimensionality disaster is highlighted. Thus, further improvement in efficiency, such as more efficient selection of representative point sets and decrease of the system dimension, will be one of main tasks in the future.

Figure 7 shows the comparison between mPDFs of system (29) in resonant state and non-resonant state. When the system is in resonance, the mPDFs of displacement and velocity are approximately the same in each degree-of-freedom. Comparing with the non-resonant case, the system (29) in resonance is very unstable and prone to vibration, which is just consistent with the reality.

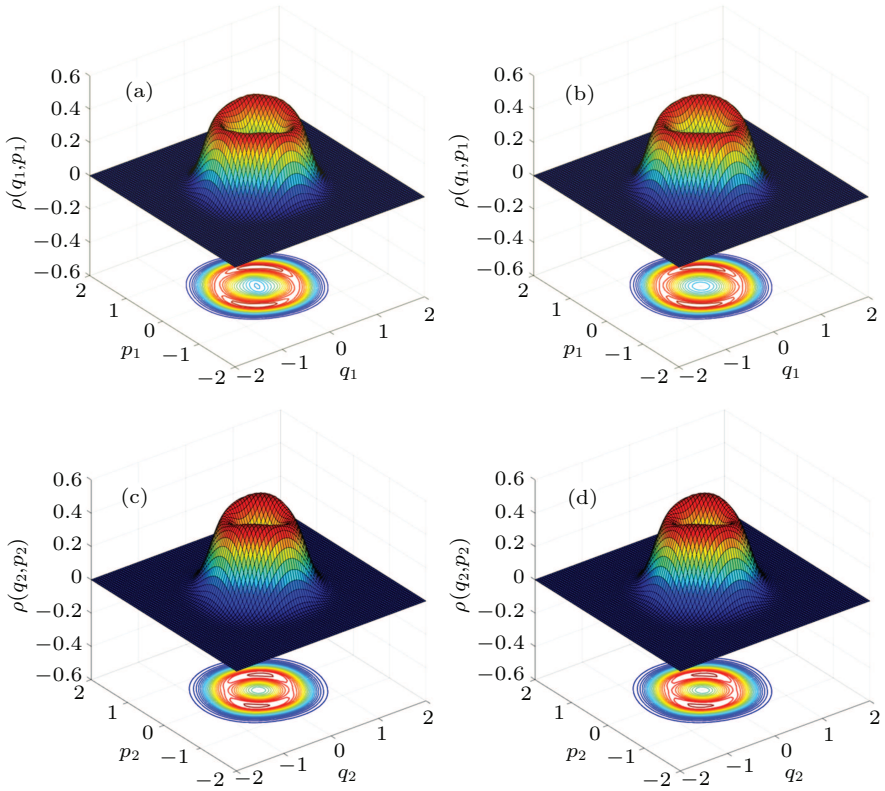


Fig. 6. Comparison among joint PDFs of system (29) in resonance, showing ((a), (c)) RBF-NN solutions and ((b), (d)) MCS results.

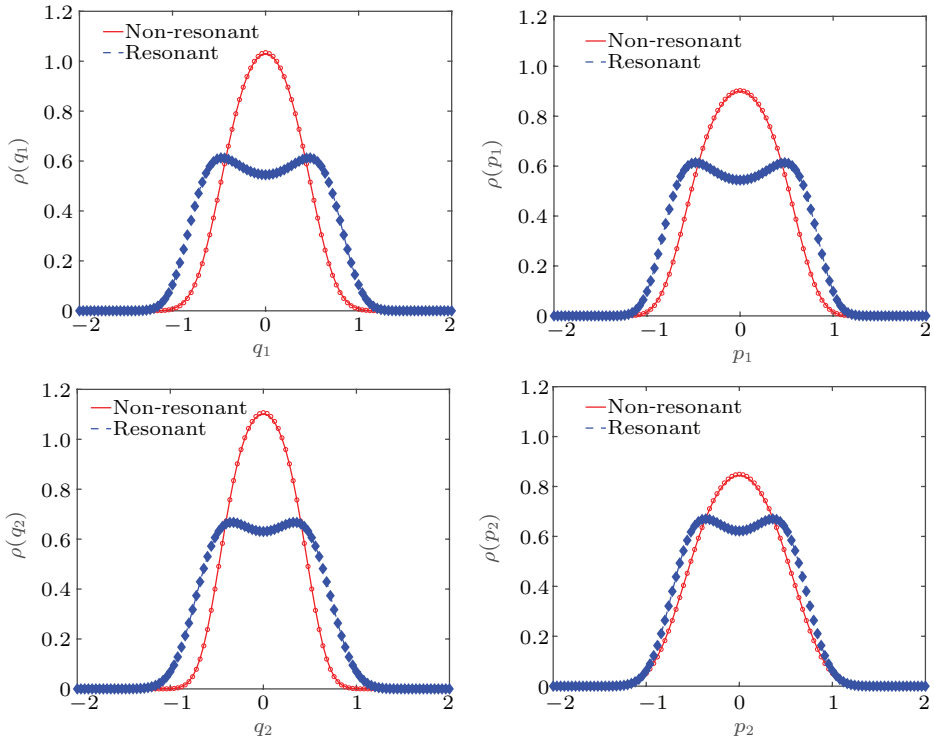


Fig. 7. Comparisons among mPDFs of system (29) in different states, with color lines denoting RBF-NN solutions, and symbols (◯, ◊) representing MCS results.

5. Conclusions

In this work, the RBF-NN scheme is generalized to predict the steady-state response of multi-dimensional quasi-Hamiltonian systems. In addition, an efficient sampling strategy is employed to help implement the algorithm and reduce the influence of dimension disaster to some extent. Two specific examples involving quasi-non-integrable system, quasi-integrable system of resonant case and non-resonant case are

studied to verify the effectiveness and efficiency of the proposed scheme by comparing the MCS results. All comparison results show that the nonlinear features of system response can be well captured by the proposed scheme, even for resonant cases. Significantly, the proposed scheme provides a new perspective in dealing with the issues involving quasi-Hamiltonian systems. The highly accurate solution of stationary PDF obtained is in the semi-analytical form, which not only can be used as a benchmark to check the accuracy of other methods, but also has important application value in the optimal structural design. The proposed scheme is promising and expected to solve much higher-dimensional issues, so that more efficient sampling strategy and matrix optimization algorithm are necessary.

Acknowledgements

Project supported by the National Natural Science Foundation of China (Grant No. 12072118), the Natural Science Funds for Distinguished Young Scholar of the Fujian Province, China (Grant No. 2021J06024), and the Project for Youth Innovation Fund of Xiamen, China (Grant No. 3502Z20206005).

References

[1] Xu W, Wang L, Feng J Q, Qian Y and Han P 2018 *Chin. Phys. B* **27** 110503
[2] Ghany H A 2014 *Chin. Phys. Lett.* **31** 60503
[3] Zhu W Q, Cai G Q and Lin Y K 1992 *IUTAM Symposium*, 1991, Turin, Italy, p. 543
[4] Zhu W Q 2006 *Appl. Mech. Rev.* **59** 230
[5] Huang Z L and Jin X L 2009 *Sci. China Ser. E-Technol. Sci.* **52** 2424
[6] Zhu W Q and Huang Z L 2001 *Int. J. Nonlinear Mech.* **36** 39
[7] Ying Z G and Zhu W Q 2000 *Int. J. Nonlinear Mech.* **35** 837
[8] Huang Z L and Zhu W Q 2000 *J. Sound Vib.* **230** 709
[9] Zhu W Q and Yang Y Q 1996 *J. Appl. Mech.* **63** 493
[10] Zhu W Q and Deng M L 2004 *J. Sound Vib.* **274** 1110
[11] Zhu W Q, Huang Z L and Suzuki Y 2001 *Int. J. Nonlinear Mech.* **36** 773
[12] Jia W T and Zhu W Q 2014 *Nonlinear Dynam.* **76** 1271
[13] Zeng Y and Zhu W Q 2010 *J. Appl. Mech.* **78** 021002
[14] Deng M L and Zhu W Q 2007 *J. Sound Vib.* **305** 783
[15] Huang Z L and Zhu W Q 2004 *Probabilist. Eng. Mech.* **19** 219
[16] Wang J L, Leng X L and Liu X B 2021 *Chin. Phys. B* **30** 60501
[17] Sun J Q, Xiong F R, Schütze O and Hernández C 2018 *Cell mapping methods* (Singapore: Springer)
[18] Er G K 2000 *Int. J. Nonlinear Mech.* **35** 69
[19] Guo S S, Er G K and Lam C C 2014 *Nonlinear Dynam.* **77** 597
[20] Zhang H, Xu Y, Liu Q, Wang X L and Li Y G 2022 *Nonlinear Dynam.* **108** 4029
[21] Zhang Y an Yuen K V 2022 *Int. J. Nonlinear Mech.* **147** 104202
[22] Xu Y, Zhang H, Li Y G, Zhou K, Liu Q and Kurths J 2020 *Chaos* **30** 13133
[23] Zio E 2013 *Monte carlo simulation: The method* (London: Springer) pp. 19–58
[24] Hirvijoki E, Kurki-Suonio T, äkäslompolo S, Varje J, Koskela T and Miettunen J 2015 *J. Plasma Phys.* **81** 435810301
[25] Chen L C and Sun J Q 2020 *Appl. Math. Mech.* **41** 967
[26] Li J Y, Wang Y, Jin X L and Huang Z L 2021 *Nonlinear Dynam.* **105** 1297
[27] Yang J N, Liu J G and Guo Q 2018 *Acta Phys. Sin.* **67** 048901 (in Chinese)
[28] Wang X Y, Wang Y, Qin X M, Li R and Eustace J 2018 *Chin. Phys. B* **27** 100504
[29] Jin L, Wang X J, Zhang Y and You J W 2018 *Chin. Phys. B* **27** 98901
[30] Luo S L, Gong K, Tang C S and Zhou J 2017 *Acta Phys. Sin.* **66** 188902 (in Chinese)
[31] Sun J C 2016 *Chin. Phys. Lett.* **33** 100503
[32] Fang P J, Zhang D M and He M H 2015 *Chin. Phys. Lett.* **32** 88901
[33] Gao S G, Dong H R, Sun X B and Ning B 2015 *Chin. Phys. B* **24** 10501
[34] Chen H, Kong L and Leng W J 2011 *Appl. Soft Comput.* **11** 855
[35] Mai-Duy N and Tanner R I 2005 *Int. J. Numer. Meth. Eng.* **63** 1636
[36] Li J Y, Luo S W, Qi Y J and Huang Y P 2003 *Neural Netw.* **16** 729
[37] Wang X, Jiang J, Hong L and Sun J Q 2022 *J. Vib. Acoust.* **144** 051014
[38] Wang X, Jiang J, Hong L and Sun J Q 2022 *Int. J. Dynam. Control* **10** 1385
[39] Er G K 2011 *Ann. Phys.* **523** 247
[40] Nelles O 2020 *Nonlinear system identification*, 2nd edn. (Cham: Springer Nature) pp. 831–891
[41] Chen J B and Li J 2008 *Int. J. Numer. Meth. Eng.* **74** 1988
[42] Zhu W Q, Huang Z L and Yang Y Q 1997 *J. Appl. Mech.* **64** 975